Light-Triggered Trafficking to the Cell Nucleus of a Cationic Polyamidoamine Functionalized with Ruthenium Complexes

Mascheroni, Luca; Francia, Valentina; Rossotti, Beatrice; Ranucci, Elisabetta; Ferruti, Paolo; Maggioni, Daniela; Salvati, Anna

Published in:
ACS Applied Materials & Interfaces

DOI:
10.1021/acsami.0c08033

Publication date:
2020

ACS APPLIED MATERIALS & INTERFACES

www.acsami.org

Research Article

Light-Triggered Trafficking to the Cell Nucleus of a Cationic Polyamidoamine Functionalized with Ruthenium Complexes

Luca Mascheroni, Valentina Francia, Beatrice Rossotti, Elisabetta Ranucci, Paolo Ferruti, Daniela Maggioni,* and Anna Salvati*

Cite This: *ACS Appl. Mater. Interfaces* 2020, 12, 34576–34587

Read Online

ACCESS | Metrics & More | Article Recommendations | Supporting Information

ABSTRACT: Strategies for endosomal escape and access to the cell nucleus are highly sought for nanocarriers to deliver their load efficiently following endocytosis. In this work, we have studied the uptake and intracellular trafficking of a polycationic polyamidoamine (PAA) endowed with a luminescent Ru complex, Ru–PhenAN, that shows unique trafficking to the cell nucleus. Live cell imaging confirmed the capacity of this polymer to access the nucleus, excluding artifacts due to cell fixation, and clarified that the mechanism of escape is light-triggered and relies on the presence of the Ru complexes and their capacity to absorb light and act as photosensitizers for singlet oxygen production. These results open up the possibility to use PAA–ruthenium complexes for targeted light-triggered delivery of genetic material or drugs to the cytosol and nucleus.

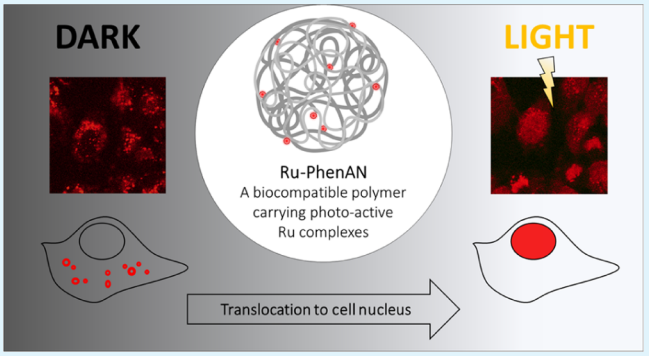

KEYWORDS: *polyamidoamines, luminescent ruthenium complexes, nuclear trafficking, endosomal escape, light-triggered escape*

INTRODUCTION

Nanomedicine holds great promise to change the way drugs are delivered to their target, owing to the use of nanosized drug carriers capable to enter cells and be trafficked intracellularly via energy-dependent pathways.[1,2] This is very different from the way most drugs reach their target, often based simply on their solubility and partition coefficients in lipids and water.[3−5] Since the very first examples of lipid-based drug carriers like Doxil,[6] research in this field has continued to be extremely active and several other products have reached the market.[7] However, it is also known that drug delivery remains rather challenging and several factors are still limiting its potential.[8−10]

Among such factors, it has emerged that most nanosized carriers entering cells via endocytosis are later trafficked along the endolysosomal pathway to the lysosomes, where the low pH and abundant proteases can degrade and destroy the internalized cargo.[5,11] This can be a dead-end for many drug carriers and their load, especially considering that in many cases drugs need to be able to reach their cellular targets in the cytosol or other cell compartments, including the nucleus. Strategies to escape the endosomes and lysosomes are being investigated via mechanisms such as the so-called proton sponge effect or by taking inspiration from toxins and viruses capable of hijacking the endo-lysosomal pathway.[11,12] For instance, for gene therapy and other therapies based on the delivery of DNA or small interfering RNA molecules, several viral and nonviral vectors have been investigated to try to deliver the genetic material to the cell nucleus or cytosol.[12]

Cationic polymers and lipids are often used for this purpose,[13−15] because of their capacity to complex the negatively charged DNA or RNA molecules while also showing to promote endosomal escape. The mechanisms by which this is achieved are often unclear and can include proton sponge effects or fusion with the endosomal membrane to release the cargo in the cytosol, among others.[16] This is often a consequence of differences in protonation levels, as the pH lowers along the endo-lysosomal pathway.[17,18] Similar endosomal escape strategies can still be limited by low efficiency as often only very few events of endosomal escape are observed and most of the material still ends in the lysosomes. In contrast, in other cases, highly cationic molecules can be limited by high toxicity because of their charge or because they may promote excessive rupture events in the endosome and lysosomes, leading ultimately to cell death.[19,20]

Among the many polymer species employed as gene delivery vectors, linear polyamidoamines (PAAs) are very interesting and

Received: May 1, 2020
Accepted: July 9, 2020
Published: July 9, 2020

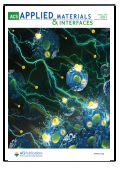

https://dx.doi.org/10.1021/acsami.0c08033
ACS Appl. Mater. Interfaces 2020, 12, 34576–34587

promising materials. They are synthetic water-soluble biodegradable polymers that can be designed to be highly biocompatible.[21,22] All of them show different charge distribution profiles as a function of pH.[23] Most PAAs have very low toxicities, with LD_{50} values in vitro 2 orders of magnitude higher than other cationic polymers, such as polyethyleneimine,[24] poly(L-lysine),[25] and polyamidoamine dendrimers (PAMAM).[26] The ability of linear PAAs to promote gene transfection in vitro was already demonstrated for some PAAs.[27,28] In addition, a linear amphoteric, but prevailingly cationic, homopolymer, named AGMA1, has also been shown to promote gene transfection in vivo[29] and to mediate the efficient delivery of siRNA in vitro.[30] More recently, another amphoteric copolymer, PhenISA,[31] derived from the same bisacrylamide (containing a carboxylic group) and functionalized with a phenanthroline pendant in its minority part was also prepared. This allowed decorating the polymer with organometallic photoluminescent Re, Ru,[31] or Ir[32] complexes, which could be exploited for photodynamic therapy (PDT).[32]

Labeling of PAAs with organometallic luminescent probes also provides many advantages in comparison to organic fluorescent dyes, such as high photostability, minimal background interference, long lifetimes, and high quantum yields. Moreover, the metal to ligand charge transfer (MLCT) absorption bands in the visible region allow the excitation of these compounds at longer wavelengths, which ensures a smaller light energy dose per cell, implying lower phototoxic effects. These effects can be maximized when excitation by two-photon absorption (TPA) is allowed.[32−34] In this field, polyimine Ru(II) complexes have been mostly investigated.[35]

Because of the prevailingly negative charge at physiological pH of the PhenISA copolymer, the internalization by HeLa cells of its Ru derivative was poor.[36] For this reason, we recently developed a new slightly cationic PAA copolymer Ru-complex (Ru−PhenAN, Chart 1), easily internalized by HeLa cells and

Chart 1. Depiction of the Structure of Polycationic Ru−PhenAN PAA Derivative

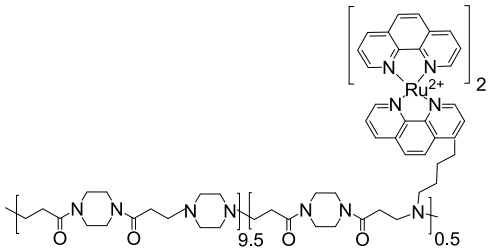

Ru-PhenAN

highly effective as a photosensitizer for PDT.[36] The polymer design and composition were optimized in order to include a phenanthroline pendant to tightly complex the ruthenium derivative and achieve good solubility while promoting cell uptake and endosomal escape.

Thus, in this work, we carefully investigated the uptake and intracellular trafficking of the linear polycationic PAA Ru−PhenAN. Interestingly, the polymer showed unique trafficking to the cell nucleus, also at concentrations not associated with toxicity. Thus, we have carried out detailed live fluorescence imaging studies to confirm the capacity to access the nucleus in living cells (in real-time). This, combined with studies on the potential impact of the cationic polymer on the cell membrane and lysosomes, has allowed us to investigate in more detail the mechanisms involved in this unique trafficking behavior.

EXPERIMENTAL SECTION

Materials. All chemicals were purchased from Sigma-Aldrich and used as received, if not otherwise specified. Ultrapure water (Milli-Q, Millipore, resistivity = 18 M Ω cm^{-2}) was used for the preparation of the aqueous solutions. *N*,*N*′-Bis(acrylamido)piperazine, 4-(4′-aminobutyl)-1,10-phenanthroline, and $Ru(phen)_2(OTf)_2$ were prepared following literature protocols.[31,37] Minimal Essential Medium (MEM), Dulbecco's modified phosphate-buffered saline (DPBS), Trypsin solution (porcine trypsin−EDTA 0.05%), and fetal bovine serum (FBS) were purchased from Gibco Thermo Fisher Scientific. Unlabeled 50 nm amino-modified polystyrene nanoparticles (diluted to 10 mg/mL in Milli-Q water) were purchased from Bangs Laboratories and used as additional controls for some of the assays performed. The primary antibody against lysosome-associated membrane protein (LAMP-1, 1 mg/mL solution) and Alexa Fluor 488-conjugated secondary antibody (2 mg/mL solution) were purchased, respectively, from Abcam and Thermo Fischer Scientific. The DNA marker 4′,6-diamidino-2-phenylindole (DAPI) was purchased from Thermo Fisher Scientific. The viability test reagents 3-(4,5-dimethylthiazol-2-yl)-2,5-diphenyltetrazolium bromide (MTT) and alamarBlue Cell Viability Reagent were purchased, respectively, from Sigma Aldrich and Thermo Fisher Scientific. LysoTracker Red DND-99 [1 mM solution in dimethyl sulfoxide (DMSO)] was purchased from Thermo Fisher Scientific. Propidium iodide (PI) and sodium azide were purchased from Sigma-Aldrich. The fluorescent oligonucleotide (ODN) was synthesized by Biomers.net, upon customer request [base sequence: 5′-ACTACTACACTAGACTAC-3′,5′-end labeled with ATTO488 fluorescent dye, purified by high-performance liquid chromatography (HPLC)]. All in vitro tests were performed using polystyrene cell culture plates purchased from Greiner. Round glass coverslips (diameter: 12 mm; thickness: 0.13 mm) were purchased from VWR.

Synthesis and Characterization of the Poly(amidoamine) PhenAN. The polymer used in this work was the same used in a previous paper[36] (M_n = 34,627 Da; M_w = 48,050 Da, PD = 1.38); yield 75%. A second preparation produced PhenAN with a minor average molecular weight (M_n = 11,912, M_w = 13,577, PD = 1.14); yield 90%. Size exclusion chromatography (SEC) traces were obtained with Toso-Haas TSK-gel G4000 PW and TSK-gel G3000 PW columns connected in series using a Waters model 515 HPLC pump equipped with a Knauer autosampler 3800, a light scattering (LS) Viscotek 270 dual detector, UV detector Waters model 486 operating at 230 nm, and a refractive index detector Waters model 2410 (mobile phase: 0.1 M Tris buffer pH 8.00; flow rate: 1 mL/min; sample concentration: 1% solutions). Dynamic LS (DLS) measurements were performed using a Malvern Zetasizer Nano ZS instrument at 25 °C, at polymer concentrations 1 mg/mL. Nuclear magnetic resonance (NMR) experiments were performed on a Bruker DRX400 spectrometer equipped with a Bruker 5 mm BBI Z-gradient probe head with a maximum gradient strength of 53.5 G/cm.

Synthesis of Polymer Complex Ru−PhenAN. PhenAN (56 mg, 0.0078 mmol of minor monomer) was dissolved in 2.5 mL of milli-Q water. $Ru(phen)_2(OTf)_2$ (6.8 mg, 0.0090 mmol) was added to the aqueous solution and mixed. Then, the solution was heated at 50 °C for 60 min in a microwave reactor, after the pH was adjusted at 6 by adding a few drops of NaOH or HCl 1 M. After the reaction was completed, the solution showed intense red color and exhibited orange luminescence when excited by 366 nm UV light. The excess $Ru(phen)_2(OTf)_2$ was removed first by treating the mixture with NaOH until pH 10, giving rise to the unsoluble product $Ru(phen)_2(OH)_2$ easily recovered by centrifugation and then by dialysis of the supernatant solution using a 10,000 molecular weight cutoff membrane. After purification, the solution showed a bright yellow color and its photoluminescence was preserved. The dialyzed solution was eventually lyophilized, affording a yellow, fluffy solid (40 mg, yield 72%). UV−vis absorption spectra were acquired on an Agilent model 8543 spectrophotometer at room temperature. Emission spectra were obtained with an Edinburgh

https://dx.doi.org/10.1021/acsami.0c08033
ACS Appl. Mater. Interfaces 2020, 12, 34576−34587

FLS980 spectrofluorometer equipped with a 450 W xenon arc lamp, and spectra were corrected for source intensity (lamp and grating) and emission spectral response (detector and grating) by standard correction curves. ^{1}H NMR (D_2O, 300 K, 9.4 T): δ 8.53 (1H), 8.50 (4H), 8.37 (1H), 8.18 (1H), 8.14 (4H, s), 8.05 (1H), 8.00 (4H), 7.93 (1H), 7.54 (1H), 7.51 (4H), 7.42 (1H), 3.57 (4H), 3.53 (4H), 2.89 (8H), 2.71 (4H).

Cell Culture. HeLa cells (from human cervix adenocarcinoma) were purchased from the American Type Culture Collection and were cultured at 37 °C with 5% CO_2 in complete medium, obtained by supplementing MEM with 10% FBS (50 mL of FBS added to 500 mL of MEM). Cultures at ∼80% confluency were routinely split into 75 cm^2 polystyrene flasks. Splitting took place every 2−3 days. Cells were used at passages up to 20 after thawing and tested monthly to exclude mycoplasma contamination.

Viability Assays. For the alamarBlue assay, cells were seeded in a 96-well plate at a density of 10,000 cells per well and grown for 24 h. Cells were then exposed to 200 μL of Ru−PhenAN solution in complete medium for 24 h; then, 20 μL of alamarBlue reagent was added to each well. After 24 h of incubation with the polymer and alamarBlue Reagent, 100 μL of the supernatant of each well was analyzed on a SPECTRAmax spectrofluorometer (excitation: 560 nm, emission 590 nm). The recorded fluorescence is proportional to the number of cells; thus, viability was calculated as the ratio between the fluorescence of the treated cells and untreated control cells (here used as a negative control) in the same conditions. For the MTT assay, the cells were seeded in a transparent 96-well plate at a density of 10,000 cells per well and grown for 24 h. The cells were then exposed to 200 μL of Ru−PhenAN in either complete medium or serum-free medium for 90 min; then, 20 μL of MTT solution (5 mg/mL in DPBS) was added to each well. After 90 min of incubation, the wells were carefully emptied and 0.2 mL of DMSO was added to each well to solubilize the dark precipitate at the bottom of the wells. The plate was analyzed on a ThermoMax microplate reader, measuring absorbance at 550 nm. As a positive control, the results obtained in an independent experiment on HeLa cells seeded and cultured under the same conditions and exposed to 50 μg/mL of cationic 50 nm amino-modified polystyrene nanoparticles for 3 h in either complete medium or serum-free medium are shown. The recorded absorbance is proportional to the number of cells; thus, viability was calculated as the ratio between the absorbance of treated cells and untreated control cells (here used as a negative control) in the same conditions.

Ru−PhenAN Uptake via Flow Cytometry. HeLa cells were seeded in a 24-well plate, at a density of 60,000 cells per well and grown for 24 h. Cells were then exposed to Ru−PhenAN in either complete medium or serum-free medium. At the end of the incubation time, cells were washed with complete medium and DPBS and then harvested by incubation with 300 μL of trypsin for 5 min at 37 °C. Trypsin was then deactivated by the addition of 700 μL of complete medium and the cells were collected and transferred into a tube. After centrifugation at 300 *g* for 4 min, the supernatant was discarded and cells were resuspended in 500 μL of DPBS for flow cytometry.

To measure uptake in energy-depleted cells, the cells were preincubated in 5 mg/mL NaN_3 in complete medium for 30 min; then, the cells were exposed to 100 μg/mL Ru−PhenAN in complete medium containing 5 mg/mL NaN_3. Additionally, the cells were preincubated at 5 °C and then exposed to Ru−PhenAN (100 μg/mL) in complete medium at 5 °C. After exposure to the polymer, the cells were washed, harvested, and suspended in 500 μL of DPBS for flow cytometry analysis.

The cells were analyzed on a BD LSR-II flow cytometer (excitation laser: 450 nm; fluorescence channel: 615/20). Data were analyzed with FlowJo software. Forward and side scattering dot plots were used to discriminate cellular debris. A minimum of 20,000 cells (unless specified differently) were acquired for each sample in order to obtain cell fluorescence distributions. In the experiments at 5 °C, it was not always possible to record 20,000 viable cells, but for all samples a minimum of 5000 cells were acquired. For all conditions, three technical replicates were prepared for each sample and results are reported as the average and standard deviation over the three replicates of the median cell fluorescence intensity.

Ru−PhenAN Uptake via Confocal Imaging. HeLa cells were seeded in a 24-well plate equipped with glass coverslips at a density of 60,000 cells per well and grown for 24 h. The cells were then exposed to Ru−PhenAN in complete medium. After exposure, the cells were washed with complete medium and DPBS, fixed, and permeabilized by incubation with ice-cold methanol for 5 min. Lysosomes were stained with a primary antibody against LAMP1 and a green Alexa Fluor 488-labeled secondary antibody; the nuclei were stained with DAPI. The cells were imaged on a Leica TCS SP8 confocal microscope equipped with a 60× oil objective (DAPI excitation: 405 nm laser; DAPI detector: 420−460 nm. Alexa Fluor 488 excitation: 488 nm laser; Alexa Fluor 488 detector: 500−550 nm; Ru−PhenAN excitation: 405 nm; Ru−PhenAN detector: 580−800 nm). The images were analyzed with ImageJ software. All series were taken using the same settings (laser power, voltage of photomultiplier tubes, gain, etc.) to allow a quantitative comparison for the different conditions. Unless differently specified, all images were acquired adjusting settings to ensure confocality.

Live Cell Imaging. HeLa cells were seeded at a density of 100,000 cells per microscope dish (35 mm glass bottom dishes, MatTek) and incubated at 37 °C in 5% CO_2 for 24 h. Then, cells were exposed to 1 mL of Ru−PhenAN at the required concentration in complete medium. The sample was imaged straight away with a DeltaVision Elite microscope. Parameters: objective 100×; laser power 10%; Ru−PhenAN excitation: 532; Ru−PhenAN emission: 576 (TRITC Channel). Alternatively, the sample was imaged with a Leica SP8 confocal microscope, opening the pinhole size to 2.0 airy units to increase the recorded signal. Images were acquired every 5 s for up to 10 min. Parameters: 60× oil-immersion objective; DAPI excitation: 405 nm laser; DAPI detector: 420−460 nm; Ru−PhenAN excitation: 405 nm; Ru−PhenAN detector: 580−800 nm.

Flow Cytometry-Based Assays. *PI Assay.* HeLa cells were seeded in a 24-well plate at a density of 80,000 cells per well and grown for 24 h. The cells were then exposed to Ru−PhenAN in either complete medium or serum-free medium for 3 h, washed once with serum-free medium, and then incubated with a PI solution (35 μg/mL in serum-free medium) for 20 min. The cells were washed with complete medium and DPBS, harvested with trypsin, and eventually resuspended in DPBS for flow cytometry analysis on a BD FACS Array (excitation laser: 532 nm; fluorescence channel: 585/42). As a positive control, untreated HeLa cells were harvested, fixed, and permeabilized by incubation with ice-cold 100% methanol for 5 min, washed with DPBS, and incubated with a PI solution (35 μg/mL in serum-free medium) for 20 min before flow cytometry analysis. Data were analyzed with FlowJo software. Forward and side scattering dot plots were used to discriminate cellular debris. A minimum of 20,000 cells (unless specified differently) were acquired for each sample in order to obtain cell fluorescence distributions. Three technical replicates were prepared for each sample and results are reported as the average and standard deviation over the three replicates of the median cell fluorescence intensity.

LysoTracker Assay. HeLa cells were seeded in a 24-well plate at a density of 80,000 cells per well and grown for 24 h. Then, cells were exposed to Ru−PhenAN in complete medium and afterwards washed with complete medium and DPBS, harvested with trypsin, and incubated with a LysoTracker solution (50 nM in complete medium) for 15 min. The cells were eventually resuspended in 100 μL of DPBS for flow cytometry analysis on a BD FACS array as detailed above. As a positive control, in an independent experiment, HeLa cells were exposed to different concentrations of cationic 50 nm amino-modified polystyrene nanoparticles for 24 h in complete medium and then incubated with LysoTracker and analyzed as detailed above.

Statistical Analysis. For all experiments, three technical replicate samples were prepared for each condition and the results are the average and standard deviation over the three technical replicates. All experiments were repeated multiple times to confirm the outcomes. In order to compare two sets of data, a Student's *t*-test was used to determine statistically significant differences: the results of the two sets of data were considered significantly different when the resulting *p*-

https://dx.doi.org/10.1021/acsami.0c08033
ACS Appl. Mater. Interfaces 2020, 12, 34576−34587

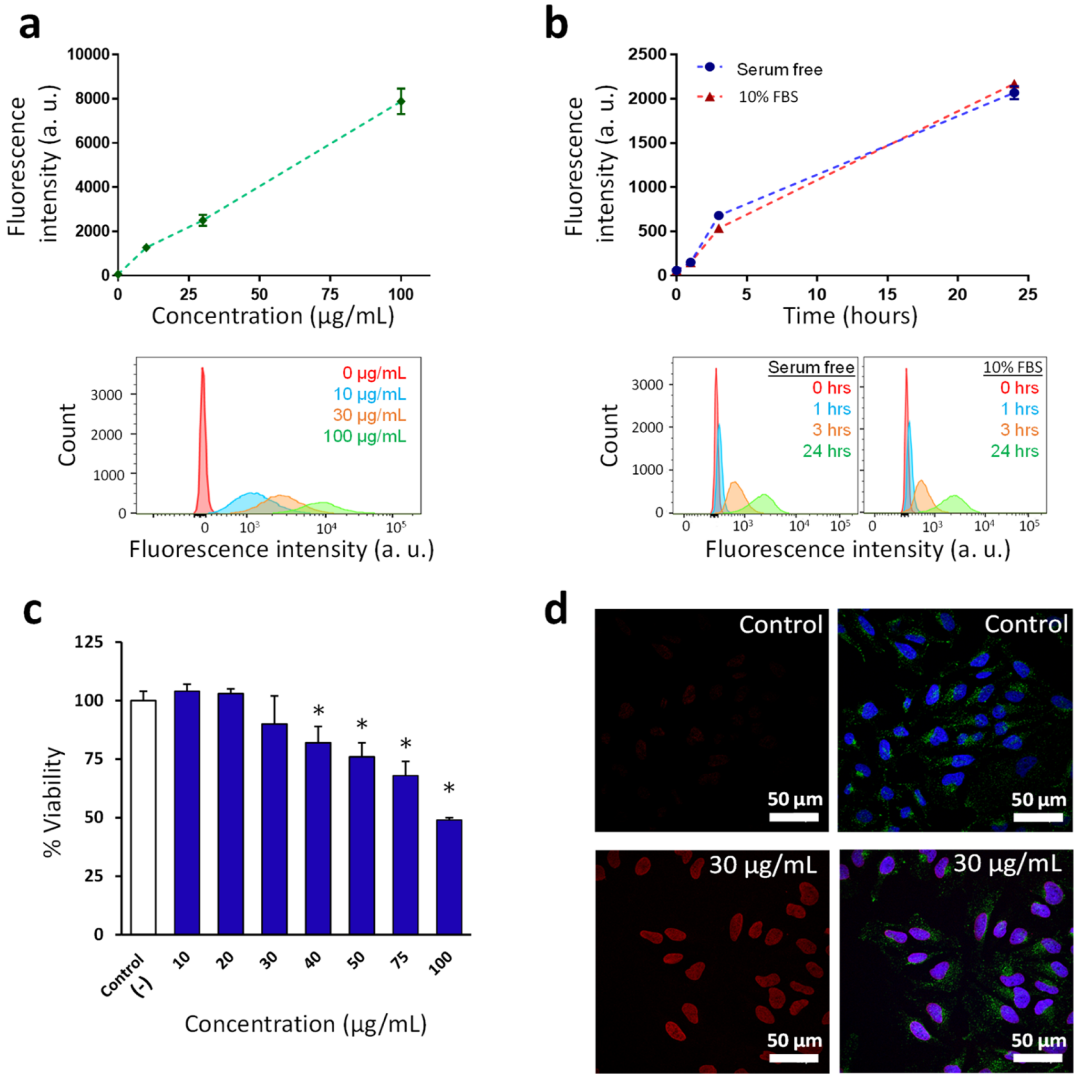

Figure 1. Uptake and viability of HeLa cells exposed to Ru−PhenAN. (a) Top panel: uptake of Ru−PhenAN in cells exposed to different concentrations of the compound in complete cell culture medium supplemented with 10% FBS (19 h of exposure). Bottom panel: examples of the corresponding cell fluorescence intensity distributions. (b) Top panel: comparison of the uptake kinetics by flow cytometry of Ru−PhenAN (30 μg/mL) in serum-free medium (blue line) and in complete cell culture medium supplemented with 10% FBS (red line). Bottom panels: examples of the corresponding cell fluorescence intensity distributions in serum-free medium (left) and in medium supplemented with 10% FBS (right). Values and error bars are the average and standard deviation over three replicates of the median cell fluorescence intensity. (c) Viability of cells (assessed via alamarBlue assay) exposed to different concentrations of Ru−PhenAN for 48 h in complete cell culture medium supplemented with 10% FBS. Values and error bars are the mean and standard deviation over three replicates. The results are expressed as a percentage with respect to untreated cells not exposed to Ru−PhenAN, here used as the negative control (−). An unpaired Student's *t*-test was used to determine statistically significant differences in comparison to untreated cells (negative control). Statistically significant differences (p-value <0.05) are indicated with an asterisk (*). (d) Intracellular accumulation of Ru−PhenAN assessed via confocal fluorescence microscopy on fixed cells. Blue: DAPI-stained nuclei; green: LAMP-1-stained lysosomes; red: Ru−PhenAN. Cells exposed to Ru−PhenAN at a concentration of 30 μg/mL for 3 h. Left panels: Ru−PhenAN channel only. Right panels: composite images of the three channels. Images of control untreated cells recorded with the same settings are also included to confirm that no signal in the Ru channel was detected.

value was <0.05. Statistically significant differences are marked with an asterisk (*).

RESULTS AND DISCUSSION

We have recently reported on the synthesis as well as the chemical and photophysical characterization of a linear polycationic PAA complexed with a luminescent tris-phenanthroline Ru complex, called Ru−PhenAN (Chart 1), which is at the basis of this investigation.[36]

The polymer can be produced with different molecular weights, depending on the time left to the reaction mixture and on the temperature. Reactions with longer times at lower temperature allow producing smaller polymers (by SEC analysis M_n = 11,912, M_w = 13,577, polydispersity index = 1.14), with respect to the one obtained previously.[36] The polymer is characterized by two mean pK_a values (pK_{a1} = 3.35, pK_{a2} = 7.40) that make the polymer cationic below a pH value of 7.40, and instead only slightly positive (about 25% of the repeating units) at physiological pH.[36] Polycationic polymers have been shown to promote endosomal escape and it is known that their overall charge and buffering capacity are at the basis of endosomal escape mechanisms promoted by the so-called proton sponge effect,[38] even though other theories and mechanisms of escape by cationic species have been proposed in the literature.[18]

https://dx.doi.org/10.1021/acsami.0c08033
ACS Appl. Mater. Interfaces 2020, 12, 34576−34587

Overall, the mild cationic character of PhenAN at physiologic pH contributes to limit its toxicity while enabling the polymer to cross cell barriers and promote escape.[39,40]

In order to label the polymer to quantify and visualize its uptake and cellular trafficking, the PhenAN copolymer was conjugated to a luminescent ruthenium-based complex (Supporting Information Figure S1). Polyimine Ru(II) complexes bearing three chelating phenanthroline ligands are very useful for cell imaging, as they also show a large absorption band in the wavelength window usually used to excite common organic fluorescent dyes employed in confocal microscopy (400−500 nm, Supporting Information Figure S1).[36] It is noteworthy that this class of complexes can also be excited by TPA, which is an important feature for biological applications because of the reduced energy associated with the employed NIR light source, thus the lower phototoxicity.

Characterization of PhenAN and Ru−PhenAN in Relevant Media. The PhenAN polymer and its Ru-based derivative Ru−PhenAN were previously characterized in water by employing several techniques such as DLS, transmission electron microscopy, and NMR to gain information about their stability and size. It is indeed well known that PAAs tend to self-assemble in water forming nanoaggregates of variable sizes.[21,31,41] The results indicated that the polymer formed aggregates of around 20 nm with a smaller fraction of objects of around 90 nm.[36]

Conversely, DLS of the polymer in saline water showed a mean hydrodynamic diameter of about 200 nm (by intensity, see Supporting Information Figure S2): neither pH changes (from 3.5 to 8.7) nor the time after the dissolution of the lyophilized polymer caused any variation of the size distribution profile, indicating good stability of the agglomerates over time.

We also characterized the polymer in PBS by nanoparticle tracking analysis (NTA, Supporting Information Figure S3). NTA can partially overcome some limitations of DLS for polydisperse samples, but for poorly scattering materials it cannot easily detect sizes below 100 nm. NTA results showed average sizes of around 120 nm in PBS and allowed us at least to exclude the presence of larger aggregates.

The dispersions of the polymer in a cell culture medium with serum were also characterized. It is known that in biological fluids, nanosized materials can become unstable because of the high ionic strength of these media,[42,43] and furthermore, they can adsorb proteins and biomolecules present in the surrounding environment.[18,44,45] It is thus important to ensure that the sample remains stable in the conditions used for cell experiments. DLS in these complex media can become extremely challenging because of the presence of the proteins, especially for polymers such as the one studied here, which already showed limited scattering when dispersed in water. Indeed, multiple peaks were determined by DLS, possibly because of limited scattering or suggesting agglomeration (data not shown). To further elucidate this, NTA was again used to (at least) exclude the presence of strong agglomeration in these conditions. The results showed a main peak shifted to slightly larger values (around 160 nm) than what was measured in PBS, possibly because of the adsorption of proteins on the polymer (see Supporting Information Figure S3). Importantly, no presence of aggregates was detected, overall suggesting that the polymer was stable also in complete cell culture medium.

Uptake and Intracellular Trafficking of Ru−PhenAN in Fixed and Live Cells. HeLa human cervical cancer epithelial cells were chosen as a common model system to study uptake and intracellular trafficking of the Ru−PhenAN polymer.

The presence of the ruthenium complex allowed quantification of uptake by cells via flow cytometry. The results showed that the polymer was internalized, and uptake increased with the polymer dose and exposure time, as commonly observed for similar materials (Figure 1a,b). We also compared the uptake of the polymer added to cells in complete medium with and serum-free medium and interestingly we found no major differences in the uptake efficiency in the two conditions (Figure 1b): it is known that the adsorption of proteins on nano-sized particles (forming the so-called nanoparticle corona) typically leads to a much lower uptake into cells in comparison to what is observed when bare nanomaterials are exposed to cells in the absence of proteins.[46−50] Thus, the fact that for this polymer no major differences in uptake levels were observed in the two conditions is rather peculiar and may suggest that proteins are only loosely associated to the polymer surface, and, because of this, they do not affect the final interactions with cells. Further studies are required to explain this observation.

Cell viability measurements after 48 h of exposure (alamarBlue assay, Figure 1c) showed little or no toxicity for cells exposed up to 30 μg/mL polymer and some toxicity at the higher concentrations tested, with 50% reduction of viability for cells exposed to 100 μg/mL polymer. It was previously shown that because of their pK_a, even at low lysosomal pH (∼4.5) PAAs comparable to the major component of Ru−PhenAN are only partially protonated; thus, they possess only a mild cationic character. This is an important feature of these polymers, which makes them typically much less toxic than many other cationic polymers, such as polylysine, that at low pH are fully protonated.[51,52]

Interestingly, confocal fluorescence microscopy of fixed cells showed accumulation of the polymer in the nucleus in all cells (Figure 1d). The same was observed also in cells without DAPI staining, thus excluding spillover of the DAPI signal in the polymer channel (Supporting Information Figure S4) and using a different microscope (Supporting Information Figure S5). Similar results were observed also in a primary cell line, namely, in human umbilical vein endothelial cells exposed to Ru−PhenAN after fixation (Supporting Information Figure S6).

Accumulation at the nuclear level was confirmed also for a second Ru−PhenAN batch (Supporting Information Figure S7), which was prepared using a smaller copolymer (∼12 kDa vs ∼30 kDa, see Experimental Section). PAAs are extremely stable in physiological conditions, being resistant to proteases and hydrolyzing very slowly in the pH range 5−7.4.[53] Thus, we can exclude that the signal observed at the nuclear level comes from smaller degradation products and even if the ruthenium moiety would detach from the phenanthroline present in the main polymer, it would fully lose its capacity to fluoresce. Additionally, we previously prepared a small ruthenium complex, analogous to that carried by Ru−PhenAN, but devoid of the polymer chain (for the sake of clarity its structure is shown in Scheme S1 of the Supporting Information), and we showed that it was not accumulating at the nuclear level,[36] even when exposing cells to a Ru complex concentration 100 times higher than the molarity of the ruthenium present in 30 μg/mL Ru−PhenAN. Thus, the ruthenium moiety alone is not able to access the nucleus. Interestingly, we also prepared a fluorescent PhenAN polymer endowed with a rhodamine pendant and lacking the ruthenium complex (see Supporting Information and Figures S8−S11 for details) and showed that in fixed cells

https://dx.doi.org/10.1021/acsami.0c08033
ACS Appl. Mater. Interfaces 2020, 12, 34576−34587

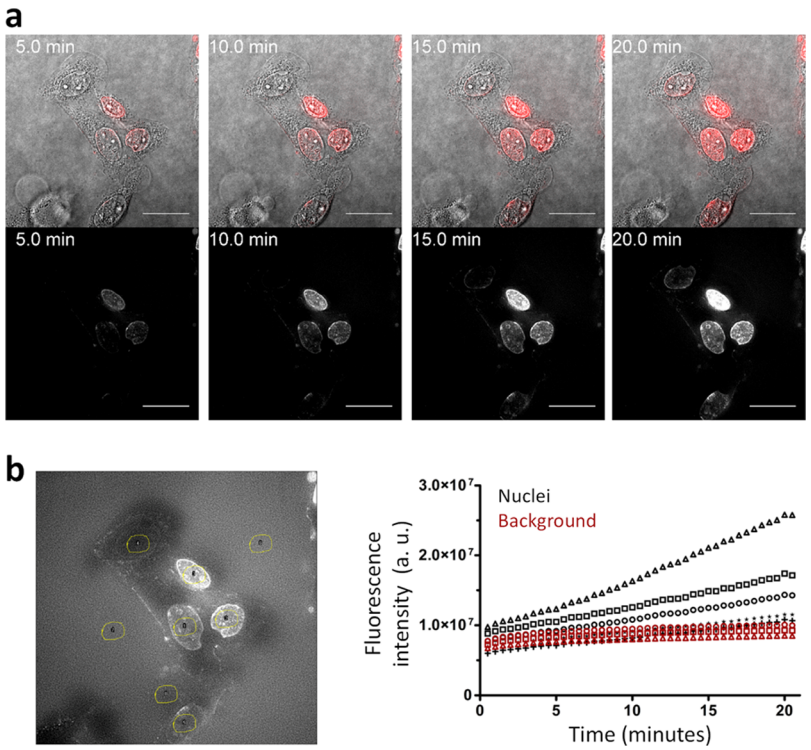

Figure 2. Cellular localization of Ru−PhenAN in live HeLa cells. HeLa cells were incubated with 30 μg/mL Ru−PhenAN in complete medium for 1 h. Then, live cells were imaged every 30 s for a total of 20 min on a DeltaVision Elite fluorescence wide field microscope. (a) Images show that the nuclear signal of Ru−PhenAN increases over time. Top: merged bright-field image and Ru−PhenAN fluorescence signal (red). Bottom: Ru−PhenAN fluorescence signal only (white). Scale bar: 25 μm. The corresponding Video S1 is included in the Supporting Information. (b) Fluorescence intensity (raw integrated density) in eight arbitrary selections of the same size taken from the image shown on the left. Left image: the areas selected for the calculation of the fluorescence intensities are indicated with yellow circles. Right graph: fluorescence intensity over time of the areas selected. When the nuclei were selected (black symbols, nuclei), an increase in signal over time was measured. When regions outside the nuclei were selected (red symbols, background), the signal remained constant over time. This quantification confirmed an increase in Ru−PhenAN fluorescence inside the nuclei upon illumination, as observed in panel a and the corresponding Supporting Video S1.

this polymer was unable to reach the nucleus and remained confined in cellular vesicles (Supporting Information Figure S12). Thus, altogether, these observations suggested that the observed signal in the nuclei is due to the nuclear accumulation of the Ru−PhenAN polymer in its entirety, and that both the main polymer chain and the ruthenium-based pendant play an important role in the capacity of Ru−PhenAN to translocate to the nucleus.

It is important to mention that for some cationic molecules,[54] chemical fixation can create artifacts, in which endosomal escape and/or accumulation at the nuclear level of positive compounds is observed solely as a consequence of the membrane damage (endosomal and/or nuclear) induced by the fixation. It is also true that some cationic objects do not show such capacity even after destabilization of membranes by fixation, as for instance we observed here for the PhenAN polymer without the ruthenium complex, labeled with rhodamine (Supporting Information Figure S12). Thus, in order to confirm the capacity of Ru−PhenAN to escape the endosomes and/or access the nucleus, we performed additional studies by live cell imaging. Interestingly, as we previously observed,[36] live cell imaging showed a progressive increase of the polymer signal at the nuclear level in individual cells after only 20 min exposure, while only a few vesicles containing the polymer could be detected (Figure 2a, with quantification of nuclear fluorescence in Figure 2b, and corresponding Supporting Video S1).

It is known that some ruthenium complexes can increase their fluorescence signal sensibly when intercalated in DNA[35,55] and that the MLCT luminescence of $Ru(phen)_3^{2+}$-like complexes can strongly be affected by the binding of the complexes to DNA strands.[56] Similar phenomena could explain or at least contribute to the observed predominance of the signal at the nuclear level. In order to test whether similar effects could be present also in our case, cellular DNA was titrated into a polymer solution and its fluorescence emission recorded after 3 h of interaction. The results (Supporting Information, Figure S13) clearly confirmed that the addition of DNA does increase the emission of Ru−PhenAN (to a level comparable to the signal recorded for a polymer solution roughly 6 times more concentrated, data not shown). It is likely that DNA condensation, together with other unique environmental conditions in the nucleus (including, for instance, lower oxygen levels and a greater stiffness with respect to the other cellular suborganelles), further increases this phenomenon in cells.

Uptake of Ru−PhenAN in Energy-Depleted Cells, Impact on Lysosomes, and the Cell Membrane. The limited presence of intracellular vesicles containing the polymer at shorter exposure times could also be interpreted as a sign of a mechanism of uptake via fusion with the cell membrane and direct access to the cytosol and later the nucleus, rather than uptake via endocytosis into endosomes and a later mechanism of endosomal escape (even though a fraction of lysosomes containing the polymer were present). In order to test this and to determine whether uptake occurred via active processes such as endocytosis, cells were depleted of energy by exposure to sodium azide or by incubation at 5 °C. The results (Figure 3)

https://dx.doi.org/10.1021/acsami.0c08033
ACS Appl. Mater. Interfaces 2020, 12, 34576−34587

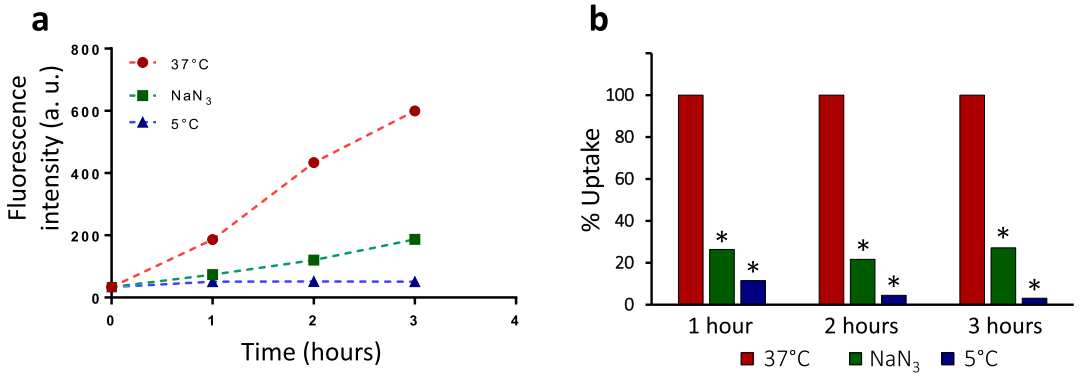

Figure 3. Uptake of Ru−PhenAN assessed via flow cytometry in standard conditions (37 °C, red) and in energy-depleted conditions. HeLa cells were depleted of their energy by supplementing the cell culture medium with 5 mg/mL NaN_3 (green) or by incubation at 5 °C (blue). (a) Uptake kinetics of Ru−PhenAN in the three conditions. Values and error bars are the average and standard deviation over three replicates of the median cell fluorescence intensity (error bars are not visible because the standard deviation is too small). (b) Same results are shown after normalization for the uptake in standard condition (37 °C). An unpaired Student's *t*-test was used to determine statistically significant differences in comparison to uptake in standard conditions. Statistically significant differences (*p*-value <0.05) are marked with an asterisk (*).

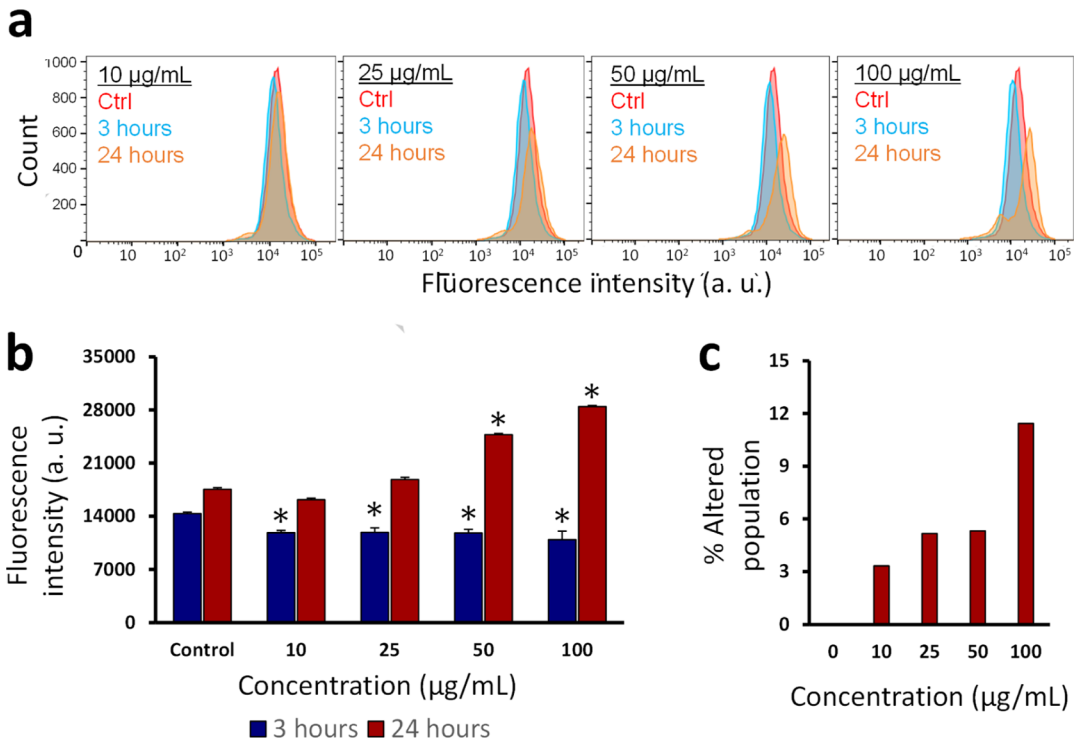

Figure 4. (a) LysoTracker intensity distributions by flow cytometry of HeLa cells exposed to different concentrations of Ru−PhenAN. At 3 h (blue distributions), the LysoTracker intensity was slighlty lower than in control untreated cells (red, negative control). At 24 h (orange), two subpopulations were visible, more and less fluorescent than control cells, respectively. (b) Corresponding LysoTracker median fluorescence intensity of cells exposed to Ru−PhenAN for 3 h (blue) and 24 h (red). Values and error bars are the average and standard deviation over three replicates of the median cell fluorescence intensity. An unpaired Student's *t*-test was used to determine statistically significant differences in comparison to the results in untreated cells. Statistically significant differences (*p*-value <0.05) are marked with an asterisk (*). As a positive control, the results obtained in cells exposed to cationic 50 nm amino-modified polystyrene nanoparticles are shown in the Supporting Information, Figure S14. (c) Corresponding percentage of cells with loss of LysoTracker staining (% altered population) after 24 h of incubation with Ru−PhenAN.

showed that uptake was blocked by energy depletion, clearly excluding the possibility for a passive uptake via a fusion mechanism with the cell membrane. It seems unlikely that other forms of active transport, such as, for instance, via active transporters present in cells for direct access of ions and small molecules to the cytosol, could be able to internalize large polymers such as the one used here. Thus, the results suggested that the polymer accumulates into cells via active uptake and is trafficked along the endo-lysosomal compartments prior to reaching the nucleus.

As some cationic polymers accumulating in the endo-lysosomal compartment are known to strongly alter the lysosomes,[57] LysoTracker staining was used to determine whether similar effects could be observed also in cells exposed to Ru−PhenAN (Figure 4). Some cationic particles and polymers can, in fact, induce damage to lysosomal membranes, leading to lysosomal swelling or rupture (associated with a

https://dx.doi.org/10.1021/acsami.0c08033
ACS Appl. Mater. Interfaces 2020, 12, 34576−34587

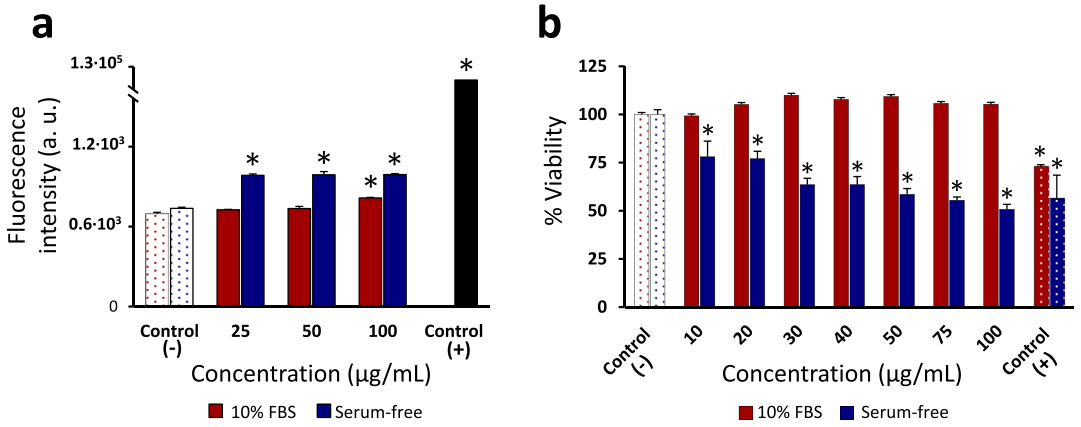

Figure 5. Impact of Ru−PhenAN on the cell membrane. (a) PI permeability test by flow cytometry after 3 h of exposure to Ru−PhenAN (30 μg/mL) in serum-free conditions (blue) and in complete cell culture medium supplemented with 10% FBS (red). As a negative control (−), untreated cells that were not exposed to Ru−PhenAN were used, and as a positive control (+), cells that were fixed and permeabilized using methanol and then stained by PI were used (see Experimental Section for details). Values and error bars are the average and standard deviation over three replicates of the median cell fluorescence intensity. (b) Viability of cells (assessed via MTT assay) exposed to different concentrations of Ru−PhenAN for 3 h in complete cell culture medium supplemented with 10% FBS (red) or in serum-free medium (blue). The results are normalized by the values obtained for untreated control cells. As a negative control (−), the viability of untreated cells not exposed to Ru−PhenAN was used and as a positive control (+), the viability of cells that were exposed for 3 h to 50 μg/mL cationic 50 nm amino-modified polystyrene nanoparticles in complete cell culture medium supplemented with 10% FBS or in serum-free medium was used. Values and error bars are the average and standard deviation of the results obtained over three replicates. An unpaired Student's *t*-test was used to determine statistically significant differences in comparison to PI fluorescence and viability in untreated cells (negative control). Statistically significant differences (p-value <0.05) are marked with an asterisk (*). The results showed that Ru−PhenAN induced some cell membrane damage only when added to cells in serum-free conditions.

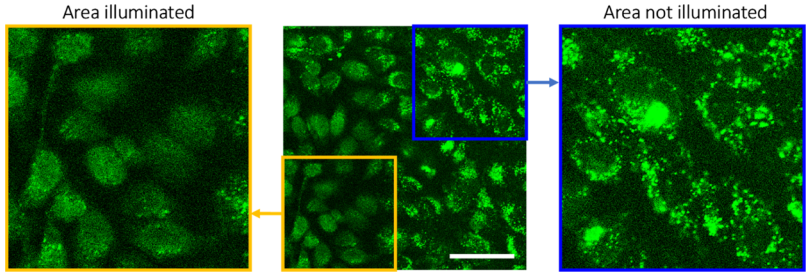

Figure 6. Cellular localization of Ru−PhenAN in live HeLa cells depends on the sample illumination. Cells were exposed to 30 μg/mL Ru−PhenAN in complete medium for 24 h in the dark and then imaged on a Leica SP8 confocal microscope, opening the pinhole size to 2.0 airy units to increase the recorded signal. Before acquiring the image, the sample area delimited by the yellow line was illuminated every 5 s for 10 min using the microscope laser, while the area within the blue line was not illuminated. Only in the illuminated area was the Ru−PhenAN signal at the nuclear level observed, whereas it remained confined in vesicles in the non-illuminated area. Scale bar: 50 μm.

strong increase of LysoTracker intensity or loss of LysoTracker staining, respectively), which could contribute to the mechanism of endosomal and lysosomal escape. Indeed, cells exposed for 24 h to amino-modified polystyrene nanoparticles were used as a positive control for similar effects and showed increased LysoTracker staining, together with a second subpopulation of cells with loss of LysoTracker staining (Supporting Information Figure S14). Instead, after 3 h of exposure to Ru−PhenAN, only a mild decrease in LysoTracker intensity was detected, possibly suggesting a small buffering effect of the polymer on the lysosomal acidity due to its positive charge. Only after 24 h of exposure, a small increase in LysoTracker intensity was observed, together with a small percentage of cells with loss of LysoTracker, possibly as a consequence of lysosomal damage or simply because of the observed toxicity at this time scale for cells exposed to these polymer concentrations (Figure 1d). Overall, however, in comparison to what was observed for other cationic nanoparticles such as the amino-modified polystyrene (Supporting Information Figure S14),[56] no major lysosomal alterations were observed. Similarly, immunostaining of the lysosomes did not show any obvious increase in lysosomal size (Figure 1c).

Given the positive charge of the polymer, we also investigated whether exposure to the polymer was associated with damage to the negatively charged cell membrane. To this aim, we measured cell membrane permeability to PI after exposure to the polymer in complete medium (containing 10% FBS) as well as in serum-free medium, where the positive charges are not screened by serum protein absorption. We stress that serum-free conditions are artificial laboratory conditions not relevant to biological applications but can be helpful in understanding nanocarrier behavior by comparison. No increase in PI permeability and no decrease in cell viability were observed after 3 h of exposure to concentrations up to 100 μg/mL in the cell culture medium containing serum (Figure 5). Interestingly, even in serum-free conditions, only a mild effect on cell membrane permeability was observed by PI staining, accompanied by a decrease in cell viability. The mild impact to the cell membrane of the bare polymer in artificial serum-free conditions further confirms its mild cationic character. This is one of the amenable features of

https://dx.doi.org/10.1021/acsami.0c08033
ACS Appl. Mater. Interfaces 2020, 12, 34576−34587

PAAs for drug delivery in comparison to other cationic species, which show much stronger damage because of the direct interaction of their bare cationic surface to the cell membrane.[56]

Light-Triggered Mechanism of Escape and Accumulation at the Nuclear Level. On the base of all these pieces of evidence (i) energy-dependent uptake (Figure 3), (ii) no obvious alterations of the acidic compartments stained by LysoTraker (Figure 4); (iii) no evident damage to the cell membrane due to the cationic character (Figure 5), we would expect to observe a more substantial number of intracellular vesicles stained by the polymer prior to the accumulation at the nuclear level observed in live cells. As this was not the case (Figure 2), we hypothesized that the light, during the observation, could have a role and trigger the release of the polmyer from intracellular vesicles. In fact, the Ru complex can act as a photosensitizer for singlet oxygen production,[36] and these are well-known cytotoxic species that can destabilize lipid membranes. To test this hypothesis, we exposed cells for 24 h to 30 μg/mL Ru−PhenAN in complete medium under standard culturing conditions in the dark. Then, we took a fast snapshot image of the live cells. This allowed us to detect that, in the dark and in the very first instants of illumination, the polymer was present in a large number of intracellular vesicles, as expected after endocytosis, and—importantly—in these dark conditions no signal at the nuclear level was visible (Supporting Information, Figure S15). Then, during the illumination, we saw a change in the subcellular localization of the emitted signal and increasing signal at the nuclear level (Video S2). The effect is evident in Figure 6, where the field of view was adjusted to allow capturing in the same snapshot both the area illuminated for 10 min (1 frame every 5 s) and a neighboring area that was not illuminated. These results clearly indicated that Ru−PhenAN remained confined in vesicles in the dark following endocytosis, while instead it accumulated in the nuclei only upon illumination. We also stress that accumulation at the nuclear level upon illumination was observed both when imaging live cells using a wide field fluorescence microscope (Figure 2) and when using a confocal microscope (as shown here in Figure 6), thus further confirming our observations even when using different instruments.

Without illumination, some degree of accumulation at the nuclear level in live cells was observed only in HeLa cells treated with much higher doses of Ru−PhenAN (300 μg/mL for 4 h) (Supporting Information, Figure S16). It is likely that in these conditions, the cationic character of the polymer enables accumulation at the nuclear level in some cells, probably simply as a consequence of the strong toxicity induced at these higher concentrations (Figure 1d), limiting their applicability overall. In contrast, upon illumination, accumulation at the nuclear level was achieved in all cells and using polymer concentrations for which no toxicity was observed. Similarly, even after the light-triggered escape and accumulation at the nuclear level, no evident signs of toxicity and cell death were observed in the imaged cells. Nevertheless, it will be important in future to further tune polymer design and illumination conditions in order to promote escape and achieve accumulation at the nuclear level while fully excluding side toxicity because of singlet oxygen production.

Finally, we performed preliminary studies on fixed cells where a fluorescently labeled ODN, here used as a model of genetic material, was complexed with increasing amounts of Ru−PhenAN to test whether the polymer was able to carry such compounds to the nucleus. In fixed cells, access to the nucleus of both the polymer and the ODN was achieved only for complexes formed at lower ODN amounts (lower ODN/Ru−PhenAN ratios, Supporting Information, Figure S17). Further studies are required to test whether the polymer shows a similar behavior on live cells.

CONCLUSIONS

Delivering drugs to the precise intracellular location of their molecular target remains one of the major barriers in drug delivery. The cell cytosol and the nucleus often need to be reached by drugs, while most nano-sized drug carriers accumulate along the endo-lysosomal pathway, where they remain trapped. Several strategies for endosomal escape and access to the nucleus are being investigated and often suffer from limited efficacy or can be accompanied by strong toxicity.

Here, we report a novel linear PAA capable to reach the cell nucleus with very high efficiency even at low concentrations, for which no toxicity is observed. This mildly cationic polymer enters cells without evident membrane damage via an energy-dependent uptake process (possibly endocytosis).

Then, upon illumination, Ru−PhenAN is capable to translocate to the nucleus, with some cells showing a polymer signal at the nuclear level already after only 20 min of exposure. The observed endosomal escape hence seems to be triggered by the illumination of the photoactive Ru complex carried by the polymer, suggesting a mechanism of escape and access to the nucleus via membrane damage due to the production of singlet oxygen by Ru. Nevertheless, the Ru complex alone is not able to move to the nucleus.[36] Thus, the mild cationic charge of the polymer is likely to facilitate the escape mechanism. At the same time, the cationic character alone is not enough to achieve accumulation at the nuclear level either, as for cells kept in the dark nuclear access was observed only after exposure to much higher polymer concentrations, probably as a consequence of the strong toxicity observed in these conditions. Finally, the results suggested that the Ru moiety not only enables a light-triggered mechanism, but is also essential to achieve the nuclear accumulation of the polymer, probably because of effects on polymer folding and conformation, since, in contrast, the same PhenAN endowed with a rhodamine moiety remained confined into intracellular vesicles without accessing the nucleus.

Overall, based on these observations, we can conclude that the ability to reach the nucleus is due to the combination of two main factors: the mild cationic character of the polymer together with the photophysical properties of the Ru complex appended to each polymer coil. Each of these two factors is necessary but not sufficient, and only when both are present it is possible to see a very efficient translocation to the nucleus.

Past studies on amphoteric PAAs suggested that these polymers could selectively damage biological membranes at low pH only,[39] possibly inducing the release of the endosome/lysosome content without a complete swelling of the intracellular vesicles. Anyhow, as previously mentioned, the detailed mechanisms of endosome membrane destabilization and escape remain poorly understood also for other polyelectrolytes such as polyethylenimine, and debate is still on-going even on the existence of the so-called proton-sponge effect and nature of other possible mechanisms.[18]

Similarly, it remains to be elucidated how such a relatively large molecule is capable to enter the nucleus. Again, we can only speculate a role for the soft linear nature of the polymer coils. Further studies are needed to fully address this aspect, as also to

https://dx.doi.org/10.1021/acsami.0c08033
ACS Appl. Mater. Interfaces 2020, 12, 34576−34587

confirm the capacity of this polymer to bring drugs or small oligos to the cytosol and/or nucleus in live cells.

Concerning the observed toxicity in the dark, we note that the measured IC_{50} dose (about 100 μg/mL) is much higher than for other polycationic non-viral vectors and more importantly access to the nucleus is achieved even at concentrations 10 times lower, for which no toxicity could be detected. Regardless of this, even though these preliminary data suggested that the light-triggered escape was not accompanied by evident toxicity, further studies are required to fully exclude side effects due to singlet oxygen production. Tuning PAA design is indeed rather easy: for instance, the addition of a minority percentage of amphoteric repeating units able to modulate the overall positive charge and further lower it could help to lower the observed toxicity and similarly the number of ruthenium moieties could be controlled in order to achieve light-triggered behavior without side toxicity. The possibility of triggering escape and access to the nucleus upon illumination opens up exciting perspectives for the use of these classes of polymers for targeted delivery. Indeed, molecular targeting by functionalization of drug carriers with antibodies and other similar targeting moieties remains highly challenging,[9] while the possibilities to engineer stimuli-responsive drug carriers is receiving increasing attention as an alternative strategy to target drugs to their destination with higher precision.[58]

■ ASSOCIATED CONTENT

Supporting Information

The Supporting Information is available free of charge at https://pubs.acs.org/doi/10.1021/acsami.0c08033.

DLS and NTA for PhenAN and Ru−PhenAN polymers, fluorescence microscopy images of fixed and live cells, Ru−PhenAN fluorescence measurements on increasing DNA, experimental details on the synthesis and characterization of PhenAN-RITC polymer, fluorescence microscopy images on live cells with and without light exposure, and confocal microscopy images of the uptake of ODN/Ru−PhenAN complexes (PDF)

Cellular localization of Ru−PhenAN in live HeLa cells incubated in 30 μg/mL Ru−PhenAN in complete medium for 1 h (AVI)

Cellular localization of Ru−PhenAN in live HeLa cells during illumination where the cells were exposed to 30 μg/mL Ru−PhenAN in complete medium for 24 h in the dark (AVI)

■ AUTHOR INFORMATION

Corresponding Authors

Daniela Maggioni − *Dipartimento di Chimica, Università degli Studi di Milano, 20133 Milan, Italy;* orcid.org/0000-0001-5201-4824; Email: daniela.maggioni@unimi.it

Anna Salvati − *Department of Nanomedicine and Drug Targeting, Groningen Research Institute of Pharmacy, University of Groningen, 9713 AV Groningen, The Netherlands;* orcid.org/0000-0002-9339-0161; Email: a.salvati.@rug.nl

Authors

Luca Mascheroni − *Dipartimento di Chimica, Università degli Studi di Milano, 20133 Milan, Italy; Department of Nanomedicine and Drug Targeting, Groningen Research Institute of Pharmacy, University of Groningen, 9713 AV Groningen, The Netherlands*

Valentina Francia − *Department of Nanomedicine and Drug Targeting, Groningen Research Institute of Pharmacy, University of Groningen, 9713 AV Groningen, The Netherlands;* orcid.org/0000-0003-4911-6832

Beatrice Rossotti − *Dipartimento di Chimica, Università degli Studi di Milano, 20133 Milan, Italy; Department of Nanomedicine and Drug Targeting, Groningen Research Institute of Pharmacy, University of Groningen, 9713 AV Groningen, The Netherlands*

Elisabetta Ranucci − *Dipartimento di Chimica, Università degli Studi di Milano, 20133 Milan, Italy;* orcid.org/0000-0002-6402-2650

Paolo Ferruti − *Dipartimento di Chimica, Università degli Studi di Milano, 20133 Milan, Italy;* orcid.org/0000-0002-5404-440X

Complete contact information is available at: https://pubs.acs.org/10.1021/acsami.0c08033

Author Contributions

L.M. performed all the experiments, except live cell imaging, which was performed by V.F., and the titration with DNA, which was performed by B.R. D.M. supervised the synthesis and characterization of the polymers and A.S. supervised the work with cells. All authors analyzed and interpreted the data. D.M. and A.S. wrote the manuscript, with contributions of all the authors. All the authors have given approval to the final version of the manuscript.

Notes

The authors declare no competing financial interest.

■ ACKNOWLEDGMENTS

Access to NTA was kindly provided by E. Frijlink and W. Hinrichs (GRIP). Imaging was performed at the UMCG Microscopy and Imaging Center, Groningen, with the support of K. Sjollema. A.S. acknowledges the University of Groningen for funding (Rosalind Franklin Fellowship). The work presented was partially supported by the European Research Council (ERC) under the European Union's Horizon 2020 research and innovation programme under grant agreement no. 637614 (NanoPaths) to A.S. D.M. kindly acknowledges the University of Milan for funding (Transition Grant 2015−2017 Linea 1A Progetto "Unimi Partenariati H2020" number 23774).

■ REFERENCES

(1) Ruoslahti, E.; Bhatia, S. N.; Sailor, M. J. Targeting of Drugs and Nanoparticles to Tumors. *J. Cell Biol.* **2010**, *188*, 759−768.

(2) Ferrari, M. Cancer Nanotechnology: Opportunities and Challenges. *Nat. Rev. Cancer* **2005**, *5*, 161−171.

(3) Rejman, J.; Oberle, V.; Zuhorn, I. S.; Hoekstra, D. Size-Dependent Internalization of Particles via the Pathways of Clathrin- and Caveolae-Mediated Endocytosis. *Biochem. J.* **2004**, *377*, 159−169.

(4) Chithrani, B. D.; Ghazani, A. A.; Chan, W. C. W. Determining the Size and Shape Dependence of Gold Nanoparticle Uptake into Mammalian Cells. *Nano Lett.* **2006**, *6*, 662−668.

(5) Salvati, A.; Åberg, C.; dos Santos, T.; Varela, J.; Pinto, P.; Lynch, I.; Dawson, K. A. Experimental and Theoretical Comparison of Intracellular Import of Polymeric Nanoparticles and Small Molecules: Toward Models of Uptake Kinetics. *Nanomedicine* **2011**, *7*, 818−826.

(6) Barenholz, Y. Doxil® - The First FDA-Approved Nano-Drug: Lessons Learned. *J. Controlled Release* **2012**, *160*, 117−134.

(7) Bobo, D.; Robinson, K. J.; Islam, J.; Thurecht, K. J.; Corrie, S. R. Nanoparticle-Based Medicines: A Review of FDA-Approved Materials and Clinical Trials to Date. *Pharm. Res.* **2016**, *33*, 2373−2387.

(8) Blanco, E.; Shen, H.; Ferrari, M. Principles of Nanoparticle Design for Overcoming Biological Barriers to Drug Delivery. *Nat. Biotechnol.* **2015**, *33*, 941−951.
(9) Wilhelm, S.; Tavares, A. J.; Dai, Q.; Ohta, S.; Audet, J.; Dvorak, H. F.; Chan, W. C. W. Analysis of Nanoparticle Delivery to Tumours. *Nat. Rev. Mater.* **2016**, *1*, 16014.
(10) Torrice, M. Does Nanomedicine Have a Delivery Problem? *ACS Cent. Sci.* **2016**, *2*, 434−437.
(11) Varkouhi, A. K.; Scholte, M.; Storm, G.; Haisma, H. J. Endosomal Escape Pathways for Delivery of Biologicals. *J. Controlled Release* **2011**, *151*, 220−228.
(12) Dominska, M.; Dykxhoorn, D. M. Breaking down the Barriers: SiRNA Delivery and Endosome Escape. *J. Cell Sci.* **2010**, *123*, 1183−1189.
(13) Mintzer, M. A.; Simanek, E. E. Nonviral Vectors for Gene Delivery. *Chem. Rev.* **2009**, *109*, 259−302.
(14) Guo, X.; Huang, L. Recent Advances in Nonviral Vectors for Gene Delivery. *Acc. Chem. Res.* **2012**, *45*, 971−979.
(15) Yin, H.; Kanasty, R. L.; Eltoukhy, A. A.; Vegas, A. J.; Dorkin, J. R.; Anderson, D. G. Non-Viral Vectors for Gene-Based Therapy. *Nat. Rev. Genet.* **2014**, *15*, 541−555.
(16) Hafez, I.; Maurer, N.; Cullis, P. On the Mechanism Whereby Cationic Lipids Promote Intracellular Delivery of Polynucleic Acids. *Gene Ther.* **2001**, *8*, 1188−1196.
(17) Benjaminsen, R. V.; Mattebjerg, M. A.; Henriksen, J. R.; Moghimi, S. M.; Andresen, T. L. The Possible "Proton Sponge" Effect of Polyethylenimine (PEI) Does Not Include Change in Lysosomal PH. *Mol. Ther.* **2013**, *21*, 149−157.
(18) Nel, A. E.; Mädler, L.; Velegol, D.; Xia, T.; Hoek, E. M. V.; Somasundaran, P.; Klaessig, F.; Castranova, V.; Thompson, M. Understanding Biophysicochemical Interactions at the Nano−Bio Interface. *Nat. Mater.* **2009**, *8*, 543−557.
(19) Shete, H. K.; Prabhu, R. H.; Patravale, V. B. Endosomal Escape: A Bottleneck in Intracellular Delivery. *J. Nanosci. Nanotechnol.* **2014**, *14*, 460−474.
(20) Lv, H.; Zhang, S.; Wang, B.; Cui, S.; Yan, J. Toxicity of Cationic Lipids and Cationic Polymers in Gene Delivery. *J. Controlled Release* **2006**, *114*, 100−109.
(21) Ferruti, P. Poly(Amidoamine)s: Past, Present, and Perspectives. *J. Polym. Sci., Part A: Polym. Chem.* **2013**, *51*, 2319−2353.
(22) Ranucci, E.; Manfredi, A. Polyamidoamines: Versatile Bioactive Polymers with Potential for Biotechnological Applications. *Chem. Afr.* **2019**, *2*, 167.
(23) Ranucci, E.; Ferruti, P.; Lattanzio, E.; Manfredi, A.; Rossi, M.; Mussini, P. R.; Chiellini, F.; Bartoli, C. Acid-Base Properties of Poly(Amidoamine)S. *J. Polym. Sci., Part A: Polym. Chem.* **2009**, *47*, 6977−6991.
(24) Boussif, O.; Lezoualc'h, F.; Zanta, M. A.; Mergny, M. D.; Scherman, D.; Demeneix, B.; Behr, J. P. A Versatile Vector for Gene and Oligonucleotide Transfer into Cells in Culture and in Vivo: Polyethylenimine. *Proc. Natl. Acad. Sci. U.S.A.* **1995**, *92*, 7297−7301.
(25) Wu, G. Y.; Wu, C. H. Receptor-Mediated in Vitro Gene Transformation by a Soluble DNA Carrier System. *J. Biol. Chem.* **1987**, *262*, 4429−4432.
(26) Eichman, J. D.; Bielinska, A. U.; Kukowska-Latallo, J. F.; Baker, J. R. The Use of PAMAM Dendrimers in the Efficient Transfer of Genetic Material into Cells. *Pharm. Sci. Technol. Today* **2000**, *3*, 232−245.
(27) Richardson, S. C. W.; Pattrick, N. G.; Stella Man, Y. K.; Ferruti, P.; Duncan, R. Poly(Amidoamine)s as Potential Nonviral Vectors: Ability to Form Interpolyelectrolyte Complexes and to Mediate Transfection in Vitro. *Biomacromolecules* **2001**, *2*, 1023−1028.
(28) Ferruti, P.; Franchini, J.; Bencini, M.; Ranucci, E.; Zara, G. P.; Serpe, L.; Primo, L.; Cavalli, R. Prevailingly Cationic Agmatine-Based Amphoteric Polyamidoamine as a Nontoxic, Nonhemolytic, and "Stealthlike" DNA Complexing Agent and Transfection Promoter. *Biomacromolecules* **2007**, *8*, 1498−1504.
(29) Cavalli, R.; Bisazza, A.; Sessa, R.; Primo, L.; Fenili, F.; Manfredi, A.; Ranucci, E.; Ferruti, P. Amphoteric Agmatine Containing Polyamidoamines as Carriers for Plasmid DNA In Vitro and In Vivo Delivery. *Biomacromolecules* **2010**, *11*, 2667−2674.
(30) Cavalli, R.; Primo, L.; Sessa, R.; Chiaverina, G.; di Blasio, L.; Alongi, J.; Manfredi, A.; Ranucci, E.; Ferruti, P. The AGMA1 Polyamidoamine Mediates the Efficient Delivery of SiRNA. *J. Drug Target.* **2017**, *25*, 891−898.
(31) Maggioni, D.; Fenili, F.; D'Alfonso, L.; Donghi, D.; Panigati, M.; Zanoni, I.; Marzi, R.; Manfredi, A.; Ferruti, P.; D'Alfonso, G.; Ranucci, E. Luminescent Rhenium and Ruthenium Complexes of an Amphoteric Poly(Amidoamine) Functionalized with 1,10-Phenanthroline. *Inorg. Chem.* **2012**, *51*, 12776−12788.
(32) Maggioni, D.; Galli, M.; D'Alfonso, L.; Inverso, D.; Dozzi, M. V.; Sironi, L.; Iannacone, M.; Collini, M.; Ferruti, P.; Ranucci, E.; D'Alfonso, G. A Luminescent Poly(Amidoamine)−Iridium Complex as a New Singlet-Oxygen Sensitizer for Photodynamic Therapy. *Inorg. Chem.* **2015**, *54*, 544−553.
(33) Galli, M.; Moschini, E.; Dozzi, M. V.; Arosio, P.; Panigati, M.; D'Alfonso, L.; Mantecca, P.; Lascialfari, A.; D'Alfonso, G.; Maggioni, D. SPIO@ SiO 2−Re@ PEG Nanoparticles as Magneto-Optical Dual Probes and Sensitizers for Photodynamic Therapy. *RSC Adv.* **2016**, *6*, 38521−38532.
(34) Licandro, E.; Panigati, M.; Salmain, M.; Vessières, A. Organometallic Bioprobes for Cellular Imaging. In *Bioorganometallic Chemistry*; Jauen, G., Salmain, M., Eds.; Wiley-VCH, 2015; pp 341−391.
(35) Campagna, S.; Puntoriero, F.; Nastasi, F.; Bergamini, G.; Balzani, V. Photochemistry and Photophysics of Coordination Compounds: Ruthenium. *Top. Curr. Chem.* **2007**, *280*, 117−214.
(36) Mascheroni, L.; Dozzi, M. V.; Ranucci, E.; Ferruti, P.; Francia, V.; Salvati, A.; Maggioni, D. Tuning Polyamidoamine Design To Increase Uptake and Efficacy of Ruthenium Complexes for Photodynamic Therapy. *Inorg. Chem.* **2019**, *58*, 14586−14599.
(37) Greaney, M. A.; Coyle, C. L.; Harmer, M. A.; Jordan, A.; Stiefel, E. I. Synthesis and Characterization of Mononuclear and Dinuclear Bis(2,2'-Bipyridine)Ruthenium(II) Complexes Containing Sulfur-Donor Ligands. *Inorg. Chem.* **1989**, *28*, 912−920.
(38) Behr, J. The Proton Sponge: A Trick to Enter Cells the Viruses Did Not Exploit. *Chimia* **1997**, *51*, 34−36.
(39) Richardson, S.; Ferruti, P.; Duncan, R. Poly(Amidoamine)s as Potential Endosomolytic Polymers: Evaluation In Vitro and Body Distribution in Normal and Tumour-Bearing Animals. *J. Drug Target.* **1999**, *6*, 391−404.
(40) Griffiths, P. C.; Paul, A.; Khayat, Z.; Wan, K.-W.; King, S. M.; Grillo, I.; Schweins, R.; Ferruti, P.; Franchini, J.; Duncan, R. Understanding the Mechanism of Action of Poly(Amidoamine)s as Endosomolytic Polymers: Correlation of Physicochemical and Biological Properties. *Biomacromolecules* **2004**, *5*, 1422−1427.
(41) Donghi, D.; Maggioni, D.; D'Alfonso, G.; Amigoni, F.; Ranucci, E.; Ferruti, P.; Manfredi, A.; Fenili, F.; Bisazza, A.; Cavalli, R. Tricarbonyl-Rhenium Complexes of a Thiol-Functionalized Amphoteric Poly(Amidoamine). *Biomacromolecules* **2009**, *10*, 3273−3282.
(42) Orts-Gil, G.; Natte, K.; Drescher, D.; Bresch, H.; Mantion, A.; Kneipp, J.; Österle, W. Characterisation of Silica Nanoparticles Prior to in Vitro Studies: From Primary Particles to Agglomerates. *J. Nanoparticle Res.* **2011**, *13*, 1593−1604.
(43) Roebben, G.; Ramirez-Garcia, S.; Hackley, V. A.; Roesslein, M.; Klaessig, F.; Kestens, V.; Lynch, I.; Garner, C. M.; Rawle, A.; Elder, A.; Colvin, V. L.; Kreyling, W.; Krug, H. F.; Lewicka, Z. A.; McNeil, S.; Nel, A.; Patri, A.; Wick, P.; Wiesner, M.; Xia, T.; Oberdörster, G.; Dawson, K. A. Interlaboratory Comparison of Size and Surface Charge Measurements on Nanoparticles Prior to Biological Impact Assessment. *J. Nanoparticle Res.* **2011**, *13*, 2675−2687.
(44) Monopoli, M. P.; Åberg, C.; Salvati, A.; Dawson, K. A. Biomolecular Coronas Provide the Biological Identity of Nanosized Materials. *Nat. Nanotechnol.* **2012**, *7*, 779−786.
(45) Röcker, C.; Pötzl, M.; Zhang, F.; Parak, W. J.; Nienhaus, G. U. A Quantitative Fluorescence Study of Protein Monolayer Formation on Colloidal Nanoparticles. *Nat. Nanotechnol.* **2009**, *4*, 577−580.
(46) Lesniak, A.; Salvati, A.; Santos-Martinez, M. J.; Radomski, M. W.; Dawson, K. A.; Åberg, C. Nanoparticle Adhesion to the Cell Membrane

and Its Effect on Nanoparticle Uptake Efficiency. *J. Am. Chem. Soc.* **2013**, *135*, 1438−1444.
(47) Lesniak, A.; Fenaroli, F.; Monopoli, M. P.; Åberg, C.; Dawson, K. A.; Salvati, A. Effects of the Presence or Absence of a Protein Corona on Silica Nanoparticle Uptake and Impact on Cells. *ACS Nano* **2012**, *6*, 5845−5857.
(48) Zhu, Y.; Li, W.; Li, Q.; Li, Y.; Li, Y.; Zhang, X.; Huang, Q. Effects of Serum Proteins on Intracellular Uptake and Cytotoxicity of Carbon Nanoparticles. *Carbon* **2009**, *47*, 1351−1358.
(49) Guarnieri, D.; Guaccio, A.; Fusco, S.; Netti, P. A. Effect of Serum Proteins on Polystyrene Nanoparticle Uptake and Intracellular Trafficking in Endothelial Cells. *J. Nanoparticle Res.* **2011**, *13*, 4295−4309.
(50) Ehrenberg, M. S.; Friedman, A. E.; Finkelstein, J. N.; Oberdörster, G.; McGrath, J. L. The Influence of Protein Adsorption on Nanoparticle Association with Cultured Endothelial Cells. *Biomaterials* **2009**, *30*, 603−610.
(51) Ranucci, E.; Spagnoli, G.; Ferruti, P.; Duncan, R.; Duncan, R. Poly(amidoamine)s with potential as drug carriers: degradation and cellular toxicity. *J. Biomater. Sci., Polym. Ed.* **1991**, *2*, 303−315.
(52) Hill, I.; Garnett, M. C.; Bignotti, F.; Davis, S. S. In Vitro Cytotoxicity of Poly(Amidoamine)s: Relevance to DNA Delivery. *Biochim. Biophys. Acta Gen. Subj.* **1999**, *1427*, 161−174.
(53) Ferruti, P.; Ranucci, E.; Sartore, L.; Bignotti, F.; Marchisio, M. A.; Bianciardi, P.; Veronese, F. M. Recent Results on Functional Polymers and Macromonomers of Interest as Biomaterials or for Biomaterial Modification. *Biomaterials* **1994**, *15*, 1235−1241.
(54) Chennoufi, R.; Bougherara, H.; Gagey-Eilstein, N.; Dumat, B.; Henry, E.; Subra, F.; Mahuteau-Betzer, F.; Tauc, P.; Teulade-Fichou, M.-P.; Deprez, E. Differential Behaviour of Cationic Triphenylamine Derivatives in Fixed and Living Cells: Triggering and Imaging Cell Death. *Chem. Commun.* **2015**, *51*, 14881−14884.
(55) Gill, M. R.; Garcia-Lara, J.; Foster, S. J.; Smythe, C.; Battaglia, G.; Thomas, J. A. A Ruthenium(II) Polypyridyl Complex for Direct Imaging of DNA Structure in Living Cells. *Nat. Chem.* **2009**, *1*, 662−667.
(56) Turro, N. J.; Barton, J. K.; Tomalia, D. A. Molecular Recognition and Chemistry in Restricted Reaction Spaces. Photophysics and Photoinduced Electron Transfer on the Surfaces of Micelles, Dendrimers, and DNA. *Acc. Chem. Res.* **1991**, *24*, 332−340.
(57) Wang, F.; Yu, L.; Monopoli, M. P.; Sandin, P.; Mahon, E.; Salvati, A.; Dawson, K. A. The Biomolecular Corona Is Retained during Nanoparticle Uptake and Protects the Cells from the Damage Induced by Cationic Nanoparticles until Degraded in the Lysosomes. *Nanomedicine* **2013**, *9*, 1159−1168.
(58) van der Meel, R.; Sulheim, E.; Shi, Y.; Kiessling, F.; Mulder, W. J. M.; Lammers, T. Smart Cancer Nanomedicine. *Nat. Nanotechnol.* **2019**, *14*, 1007−1017.

https://dx.doi.org/10.1021/acsami.0c08033
ACS Appl. Mater. Interfaces 2020, 12, 34576−34587